

DYNAMICS AND CONTROLS OF A CONCEPTUAL JOVIAN MOON TOUR SPACECRAFT*

Marco B. Quadrelli[†], Edward Mettler[‡], Jerry K. Langmaier[§]

Abstract

The dynamics and control challenges presented by a conceptual Jovian Moon Tour spacecraft are summarized in this paper. Attitude and orbital dynamics interactions are present due to the designed low-thrust trajectory, and controls structure interactions are also present due to the non-collocated sensor-actuator pairs on board the flexible spacecraft. A finite-element based simulation model is described which is capable of handling the complex orbital and attitude dynamics arising during the low-thrust spiraling maneuvers of the spacecraft. A few numerical simulations demonstrate that some of the challenges hitherto identified can be faced via integrated dynamics and control analysis, and that reasonable assessments of the pointing performance can be made.

Introduction

NASA is developing plans for an ambitious mission to orbit three planet sized moons of Jupiter - Callisto, Ganymede and Europa - which may harbor vast liquid oceans beneath their icy surfaces. These plans had their genesis in a study conducted in 2002 of a Jovian Icy Moon Tour (JIMT) mission**. This objective of the JIMT mission study was to design a spacecraft to explore the three icy moons and investigate their makeup, their history and their potential for sustaining life. To do so, NASA looked at how a nuclear reactor could enable long-duration deep space exploration. It was found that a nuclear fission reactor could produce unprecedented amounts of electrical energy to significantly improve scientific measurements, mission design options, and telecommunications capabilities. The proposed JIMT mission would incorporate a form of electric propulsion called ion propulsion, which would be powered using a nuclear fission reactor and a system for converting the reactor's heat to electricity. Figure 1 depicts a conceptual spacecraft configuration developed as part of the JIMT study.

For such a mission, attitude and orbital dynamics interactions are present due to the low-thrust trajectory design, and controls structure interactions are also involved due to the non-collocated sensor-actuator pairs. These are significant challenges to the dynamicist. We outline these interactions, as they were understood at the time of the 2002 study, in

* This research was carried out at the Jet Propulsion Laboratory, California Institute of Technology, under a contract with the National Aeronautic and Space Administration, and was concluded prior to establishment of the NASA's Project Prometheus, the Nuclear Systems Program, in 2003.

[†] Senior Engineer, Mail Stop 198-326, Guidance and Control Analysis Group, Jet Propulsion Laboratory, California Institute of Technology, 4800 Oak Grove Drive, Pasadena, CA 91109-8099, Marco.B.Quadrelli@jpl.nasa.gov

[‡] Senior Engineer, Mail Stop 198-138, Guidance and Control Analysis Group, Jet Propulsion Laboratory, California Institute of Technology, 4800 Oak Grove Drive, Pasadena, CA 91109-8099

[§] Senior Staff Engineer, Mail Stop 198-105, Avionics Systems and Technology Division, Jet Propulsion Laboratory, California Institute of Technology, 4800 Oak Grove Drive, Pasadena, CA 91109-8099

** Within Project Prometheus, the Jovian Moon Tours study has evolved into what is now referred to as the "Jupiter Icy Moons Orbiter", or JIMO, mission. The work in this paper is not reflective of studies and designs more recent activities within the JIMO Project Office, which was established shortly after completion of the Jovian Moon Tour Study.

the paper. The dynamics and controls challenges presented by the Jovian Moon Tour spacecraft are also described in this paper. A simulation model is described which is capable of handling the coupled orbital and attitude dynamics arising during the spiraling maneuvers of the spacecraft and the tight pointing requirements needed for science when in orbit around the Jovian moons. Multibody dynamic models for control of the scan platform articulation and of the spacecraft flexibility using finite elements are also described. Numerical simulations of the slew to gravity gradient stabilized mode and of the nadir pointed attitude dynamics around Europa demonstrate that some of the challenges hitherto identified can be faced via computational analysis, and reasonable assessments of the pointing performance and sensor and actuator selection can be made.

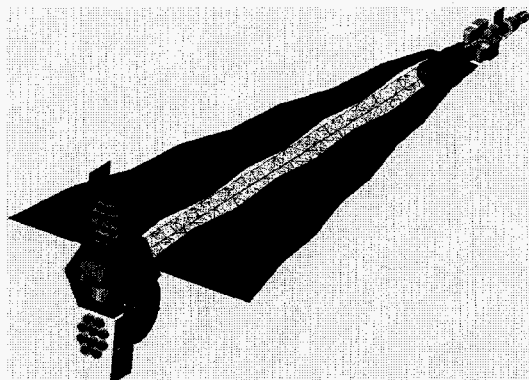


Figure 1. The proposed Jovian Moon Tour Spacecraft.

Spacecraft Attitude Control Functions

In this section, we summarize the spacecraft's main attitude control functions. Inertial measurement units (IMU) would provide body rate information. Star cameras would provide the absolute attitude reference and calibrate the IMU gyro bias drifts. IMUs would also propagate absolute attitude between star tracker updates.

Attitude Control by RCS

Three-axis stabilization would be carried out by a hydrazine reaction control system (RCS) during all coast (defined as the cruise when ion propulsion system is off) modes during launch vehicle injection, cruise, and JIMT would be using 8 fore and 8 aft coupled 4.50 N thrusters. The control law would likely be a programmable rate/position deadband limit cycle if the power conversion Brayton turbines are zero net momentum. If the net angular momentum is not zero, control law would have to be a limit cycle for pitch axis, and precession rate control for roll/yaw axes.

Attitude/Thrust Vector Control (TVC)

During powered flight with electric propulsion (EP) using xenon ion thrusters, the combined functions of delta-V and thrust vector control would be performed by the trajectory path guidance control laws. Two boom mounted EP arrays (pods) each would be articulated by gimbaling the pods in 2 degrees of freedom to produce pitch and yaw moments that null the spacecraft body rates and drive the net thrust vector through the spacecraft's center of mass. The gimballed EP arrays would also provide spacecraft roll axis control moments by coordinated 2 degree of freedom articulation. The TVC EP system would have the capability of performing continuous coplanar spiral pitch turns during planetary escape and capture maneuvers. The TVC EP system would also be able to perform uncoupled turns for plane change delta-V maneuvers. In the event of power reduction from the reactor, or imbalance turbine angular momentum being injected into the system, attitude control would have to be re-established during thrust vectoring, and this event will induce significant attitude-translation coupling.

JIMT Orbit Orientation Control

At reaching final orbit altitude the EP would be turned off and the spacecraft would be pitched up by the RCS to orient the long axis (reactor end) to zenith in the local vertical-local horizontal (LVLH) coordinate system. Yaw would be aligned with the orbit velocity vector. Pitch would be aligned normal to the orbit plane. This would place the spacecraft in a gravity gradient stable attitude with the gimbale science module pointing to nadir. The gravity gradient oscillations (librations) would be damped by the reaction wheels during science operations, when the RCS will be turned off. Since the librations are symmetric there should be little if any momentum build-up on the reaction wheels and very infrequent need to unload by the RCS.

Science Pointing Control

High resolution imaging science drives the vehicle's pointing stability. Scientific instrumentation (cameras, plasma wave antennas, gravity experiments, magnetometer boom) would be mounted on the spacecraft bus as well as on the two-degree of freedom articulated scan platform. The science platform would be mounted on a motorized gimbal at its center of mass of the science module. The platform would have its geometric center at the gimbal axes intersection. The gimbal range of travel in two axes would be +/- 45 degrees. The gimbal would be offset from the engineering module by a stiff stub boom (~ 1 meter along roll axis. The science module would contain redundant IMU's and star trackers. All imaging science cameras and other detectors requiring articulation would be on the science platform and aligned with the IMU/tracker on a common optical bench. In addition to being a massive (>20,000 kg), large (~30 meters long), flexible spacecraft, the JIMT vehicle would also host the nuclear reactor and power converters (Brayton turbines spinning at more than 30,000 rpm are part of the power conversion system). Fluid loops would also run through the radiator shield. This means that several sources of angular momentum exist, which have to be managed accordingly in order not to corrupt the science measurements.

Telecom Downlink Pointing

High data rates drives use of Ka-band science downlink. Articulation of the ~3 meter Ka-band boom mounted reflector would be done by a two-axis motorized gimbal providing +/- 90 degrees range of travel in each axis with shaft encoder feedback. The Ka-band required line of sight precision is not feasible by purely predictive (open-loop) pointing. A closed loop control would then be needed based on an uplink beacon acquired by either a monopulse detector or an adaptive feed on the antenna, and the beacon boresight offset is output by the detector and fed as two axis error signals for the gimbal loops to null.

Assumptions on Spacecraft Mass Properties, Orbit, and Configuration

Table 1 shows the parameters of the assumed orbit at Europa. Mass properties of deployed configuration are computed from a preliminary finite element model. These are shown in Table 2. However, simulation studies are carried out using a rigid vehicle model. Table 3 shows the location and direction of the thruster forces in the spacecraft body frame.

Moon	Europa
altitude	152 km
eccentricity	0.022
Inclination	100.5 degrees
Gravitational parameter Europa	$3.202733759136212e+12 \text{ m}^3/\text{s}^2$
Gravitational parameter Jupiter	$1.266865343445600e+17 \text{ m}^3/\text{s}^2$
Third body effects	Jupiter
J2 Europa	1.911786939700060e-04
J2 Jupiter	1.469629661121321e-02
J3 Europa	-6.404662179226613e-05
J3 Jupiter	4.498228966045162e-07
Distance from Sun	5.202803 AU
Orbital frequency	1.2704e-004 rad/s
Orbital period	7.8715e+003 s

Table 1. Assumption of orbital parameters for simulation study.

I_{pitch}	9.4987e+005 [kg m ²]
I_{roll}	1.5850e+004 [kg m ²]
I_{yaw}	9.5013e+005 [kg m ²]
Total SC Mass in science orbit	15105 [kg] after 12000 kg Xenon depletion
Exposed SC area	120 [m ²]
Center of Mass from first node	[0;0;5.3278] [m]
Vector from center of mass to bus	[0;0;-5.0831] [m]
Vector from center of mass to reactor	[0;0;14.9169] [m]
Center of Gravity from origin of ORF	[0;0;-0.0083] [m]
Assumed center of pressure	2 meters aft from CM
Ion Pods centroid location from SC com	[+/-4.0;0;-5.0831] [m]

Table 2. Assumption of JIMT mass properties for simulation study.

	Location wrt. Center of mass [m]			Components of thrust direction wrt. SC body axes		
Ion engine bank	0	5.0831	4.000	0	1	0
	0	5.0831	-4.000	0	1	0
RCS on bus end	-0.7071	5.0831	0.7071	0	0	1
	0.7071	5.0831	0.7071	0	0	1
	0.7071	5.0831	0.7071	1	0	0
	0.7071	5.0831	-0.7071	1	0	0
	0.7071	5.0831	-0.7071	0	0	-1
	-0.7071	5.0831	-0.7071	0	0	-1
	-0.7071	5.0831	-0.7071	-1	0	0
RCS on reactor end	-0.3536	-14.9169	0.3536	-1	0	1
	0.3536	-14.9169	0.3536	-1	0	1
	0.3536	-14.9169	0.3536	1	0	0
	0.3536	-14.9169	-0.3536	1	0	0
	0.3536	-14.9169	-0.3536	0	0	-1
	-0.3536	-14.9169	-0.3536	0	0	-1
	-0.3536	-14.9169	-0.3536	-1	0	0

Table 3. Thruster Locations in the spacecraft's body frame.

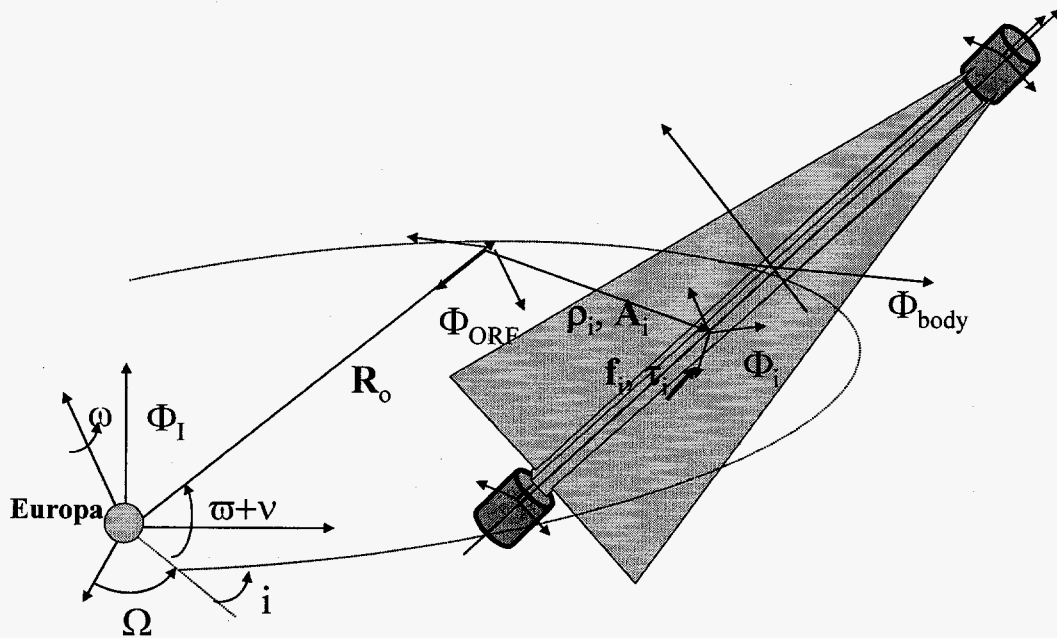


Figure 2. Geometric Description of JIMT Simulation Model.

Initial Nodal Coordinates in ORF [m]

X	Y	Z
-0.0000	0.0000	5.3278
-0.0000	0.0000	4.3278
-0.0000	0.0000	3.3278
-0.0000	0.0000	2.3278
-0.0000	0.0000	1.3278
-0.0000	0.0000	0.3278
0.0000	-0.0000	-0.6722
0.0000	-0.0000	-1.6722
0.0000	-0.0000	-2.6722
0.0000	-0.0000	-3.6722
0.0000	-0.0000	-4.6722
0.0000	-0.0000	-5.6722
0.0000	-0.0000	-6.6722
0.0000	-0.0000	-7.6722
0.0000	-0.0000	-8.6722
0.0000	-0.0000	-9.6722
0.0000	-0.0000	-10.6722
0.0000	-0.0000	-11.6722
0.0000	-0.0000	-12.6722
0.0000	-0.0000	-13.6722
0.0000	-0.0000	-14.6722

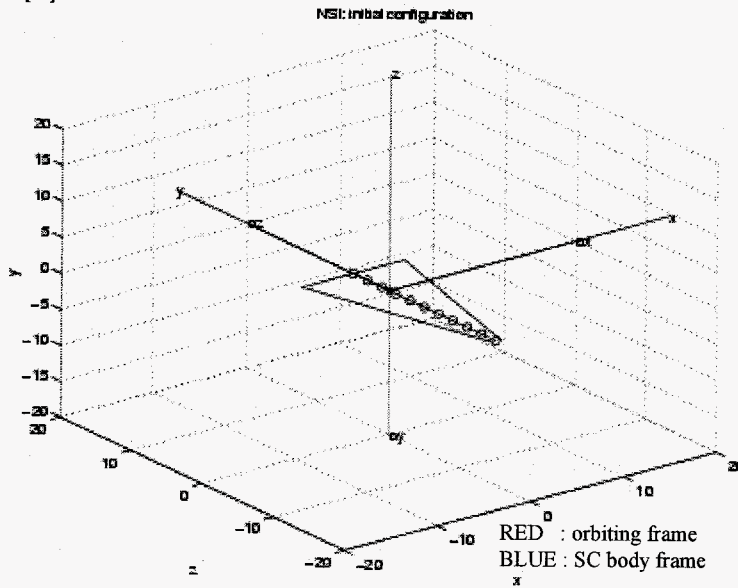


Figure 3. Flexible Boom Nodal Coordinates.

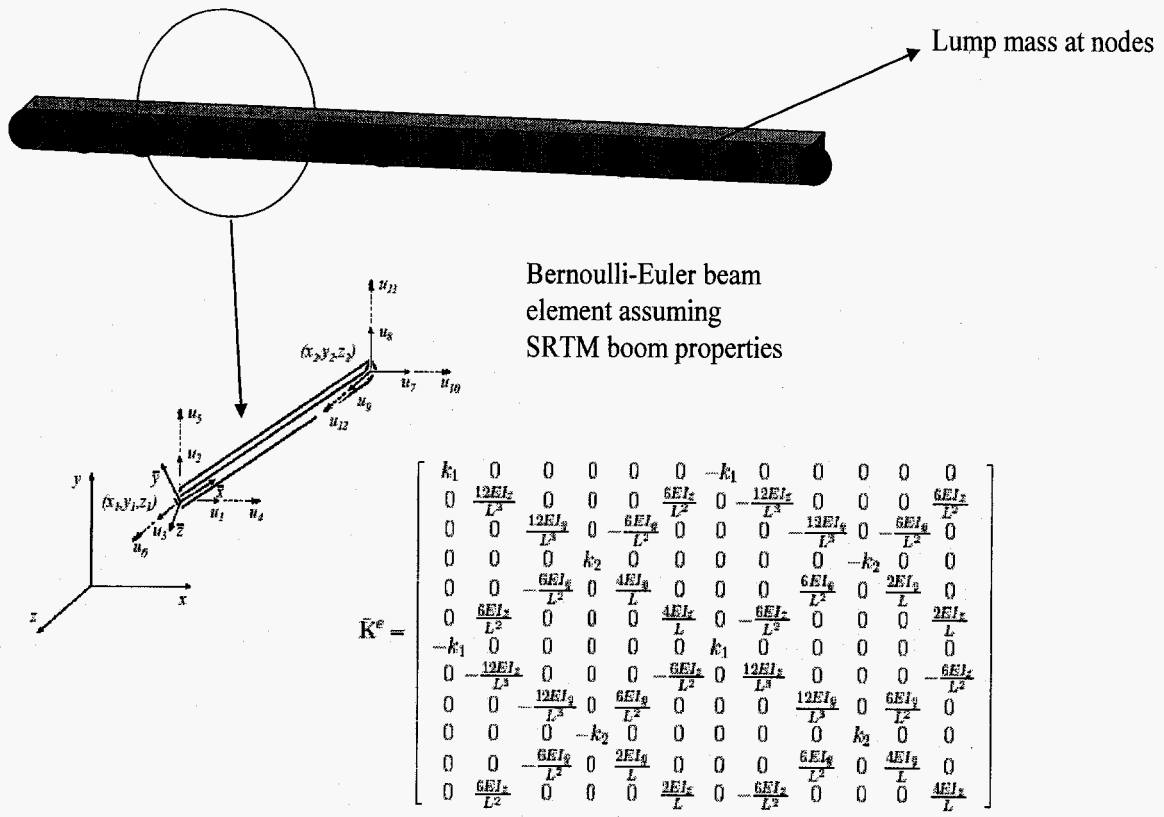


Figure 4. Flexible Spacecraft Model using a Bernoulli-Euler beam.

Modal frequencies [Hz] with rotors locked:

- 0
- 0
- 0
- 0
- 0
- 0
- 0.2016
- 0.8734
- 0.8734
- 2.0388
- 2.0388
- 2.2017
- 2.7281
- 2.7324
- 2.7324
- 2.8851
- 2.8851
- 3.5250
- 3.5250
- 4.4497
- 4.4497
- 5.6836
- 5.6836
- 6.9955
- 6.9955
- 8.2869

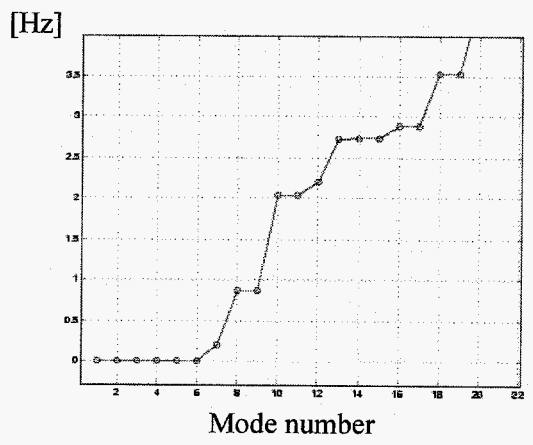


Figure 5. Flexible Spacecraft Modal Characteristics.

Spacecraft equations of motion

The equations of motion of the entire system will be derived in this section. We introduce the Europa-centric inertial reference frame Φ_1 , X pointing toward the vernal equinox, Z toward the North Pole, and Y completes the right handed reference frame, and the orbiting reference frame F_{ORF} , which we use to describe the near field dynamics of the spacecraft relative to its orbit. We refer to Fig. 2. This reference frame is attached to a point that follows a Keplerian orbit around the primary body. The body-fixed reference frame is defined as: the x-body directed from the bus towards the reactor, the y-body axis directed from the bus toward the rightmost ion engine pod, the z-body axis completes the right-handed triad. The motion of the system is described with respect to a local vertical-local horizontal (LV-LH) orbiting reference frame $(x,y,z) = \Phi_{ORF}$ of origin O_{ORF} which rotates with mean motion Ω and orbital semi-major axis R_0 , z along the local vertical, x toward the flight direction, and y in the orbit normal direction. When the spacecraft's attitude is displaced from the attitude of the Φ_{ORF} frame, the pitch angle is defined as the angle between the body-fixed X axis and the z-axis in the plane of the orbit, the yaw angle is defined as the out-of-plane angle between the body-fixed X axis and orbit plane, and the roll axis is defined as the angle around the body-fixed X axis. The orbital geometry at the initial time is defined in terms of its six orbital elements, and the orbital dynamics equation for point O_{ORF} is propagated forward in time under the influence of the gravitational field of Europa. The origin of this frame coincides with the initial position of the center of mass of the system, and the coordinate axes are z along the local vertical, x toward the flight direction, and y in the orbit normal direction. The orbit of the origin of Φ_{ORF} is defined by the six orbital elements a (semimajor axis), e (eccentricity), i (inclination), Ω_L (longitude of ascending node), ω (argument of perigee), ν (true anomaly), and time of passage through periapsis. From Fig. 1, the position vector of a generic structural point with respect to O_{ORF} is denoted by ρ_i , and we have $\mathbf{r}_i = \mathbf{R}_0 + \rho_i$. We define the state vector as $\mathbf{X} = (\mathbf{R}_0, \mathbf{V}_0, \rho_1, \mathbf{q}_1, \mathbf{v}_1, \omega_1, \dots, \rho_N, \mathbf{q}_N, \mathbf{v}_N, \omega_N, \theta_{w1}, \theta_{w2}, \theta_{w3}, \omega_{w1}, \omega_{w2}, \omega_{w3})^T$. The kinematics equations are as follows:

$$\begin{aligned} \mathbf{v}_i &= \dot{\rho}_i \\ \boldsymbol{\omega}_i &= \Gamma(\mathbf{q}_i) \dot{\mathbf{q}}_i \\ \boldsymbol{\omega}_w &= \dot{\boldsymbol{\theta}}_w \end{aligned} \quad (1)$$

where $\Gamma(\mathbf{q}_i)$ is the mapping from attitude parameters to angular velocity vector, and θ_w are reaction wheel angles. The translation kinematics and dynamics equations of a point mass of mass m in a general orbit are:

$$\ddot{\boldsymbol{\rho}} = -\ddot{\mathbf{R}}_0 - \dot{\boldsymbol{\Omega}} \times \boldsymbol{\rho} - \boldsymbol{\Omega} \times \boldsymbol{\Omega} \times \boldsymbol{\rho} - 2\boldsymbol{\Omega} \times \dot{\boldsymbol{\rho}} + \ddot{\mathbf{r}} \quad (\text{near field}) \quad (2)$$

$$\ddot{\mathbf{r}} = -\mu_E \frac{\mathbf{r}}{|\mathbf{r}|^3} + \frac{\mathbf{f}_a + \mathbf{f}_s + \mathbf{f}_3}{m} \quad (\text{far field}) \quad (3)$$

$$\ddot{\mathbf{R}}_0 = -\frac{\mu_E}{|\mathbf{R}_0|^3} \mathbf{R}_0 + \frac{\mathbf{f}_{pert} + \mathbf{f}_{J_2} + \mathbf{f}_{J_3}}{m} \quad (\text{ORF orbital dynamics}) \quad (4)$$

where: $\boldsymbol{\rho}$ = relative position vector of body i with respect to ORF, \mathbf{R}_0 = orbital radius vector to origin of ORF, $\boldsymbol{\Omega}$ = orbital rate, μ_E = Jovian moon gravitational parameter, \mathbf{f}_a = thruster actuation force vector, \mathbf{f}_s = solar pressure force vector, \mathbf{f}_3 = third-body forces vector, m = spacecraft mass with rotors added, and \mathbf{f}_{pert} , \mathbf{f}_{J_2} , \mathbf{f}_{J_3} = resultants of higher order gravitational terms from the primary acting on the entire system as an extended body. Eq.(4) describes the Keplerian orbital dynamics. The rotational dynamics equations of a spacecraft with a gyroscopic distribution about its center of mass are:

$$\mathbf{J}\dot{\boldsymbol{\omega}} + \sum_i \dot{\mathbf{H}}_i^w + \boldsymbol{\omega} \times \left(\mathbf{J}\boldsymbol{\omega} + \sum_i \mathbf{H}_i^w \right) = \mathbf{g}_e + \mathbf{g}_a \quad (5)$$

$$\dot{\mathbf{H}}_i^w = -\mathbf{g}_{w_i} \quad (i=1, \dots, \text{number of rotors}) \quad (6)$$

where: Δ = modal matrix, Λ = matrix of natural frequencies (diagonal), $\mathbf{M}_{e\omega}$ = modal inertia matrix of coupling of deformation degrees of freedom with rotor degrees of freedom, $\mathbf{M}_{\omega\omega}$ = rotor inertia matrix, \mathbf{G}_{ee} = gyroscopic coupling matrix, \mathbf{D}_{ee} = modal damping matrix, \mathbf{f}_{ee} = external forces on boom nodes (includes thruster and reactor control forces), \mathbf{f}_w = torques on rotors.

Figure 3 depicts the flexible boom nodal coordinates used for the finite element model of the spacecraft, which is shown in Figure 4 using the properties of a Bernoulli-Euler beam element. Figure 4 also shows the stiffness matrix of the Bernoulli-Euler segment used in the finite element model. Figure 5 summarizes the modal frequencies obtained by locking all rotors on the spacecraft, when the control system is operated in an open loop mode.

Interaction between orbital and attitude dynamics

In this section, we describe the effect of the attitude dynamics on the orbital dynamics and of the orbital dynamics on the attitude dynamics of the vehicle. The low-thrust propulsion system results in orbital trajectories which tend to be open spirals, rather than pure Keplerian orbits [Ref. 3]. To achieve these non-keplerian trajectories, the thrust vector control system must drive the spacecraft attitude dynamics through the appropriate ion engine pod gimbal angles, which in turn must be operated in a way that minimizes the translation-rotation coupling and the dynamic back-reaction onto the rest of the vehicle. Since this coupling cannot be eliminated, an interaction exists between the orbital and the attitude dynamics of the vehicle.

The kinetic energy of an extended rigid body in a general orbit around a planet can be written as:

$$T = \frac{1}{2} m \left(\dot{R}_0^2 + \frac{1}{2} R_0^2 \mathbf{o}_3^T \tilde{\Omega} \tilde{\Omega} \mathbf{o}_3 - 2 R_0 \dot{R}_0 \mathbf{o}_3^T \tilde{\Omega} \mathbf{o}_3 \right) + \frac{1}{2} \boldsymbol{\omega} \cdot \mathbf{J} \boldsymbol{\omega} \quad (12)$$

where \mathbf{o}_3 represents the unit vector in the nadir direction (vertical down), $\tilde{\Omega} = \tilde{\Omega}(\dot{\Omega}_L, \dot{i}, \dot{\omega}_p)$ is the vector of orbital angular velocity dependent on the time rates of the longitude of the ascending node Ω_L , the mean anomaly M , and the argument of perigee ω_p . Similarly, the gravitational potential energy of the spacecraft can be written, to second order in the displacements, as:

$$U = -\frac{\mu m}{R_0} - \frac{\mu}{2R_0^3} [\text{trace}(\mathbf{J})\mathbf{I} - 3\mathbf{o}_3 \cdot \mathbf{J} \cdot \mathbf{o}_3] \quad (13)$$

The perturbation force on an extended body orbiting around a spherical primary, caused by the extended inertia distribution of the body, can be written to second order in the normalized spacecraft size as [Ref. 1]:

$$\mathbf{f}_{pert} = \frac{3\mu}{2R_0^4} \left\{ [\text{trace}(\mathbf{J})\mathbf{I} + 2\mathbf{J}] \cdot \mathbf{o}_3 - 5(\mathbf{o}_3 \cdot \mathbf{J} \cdot \mathbf{o}_3) \mathbf{o}_3 \right\} \quad (14)$$

This perturbation force results in an acceleration applied to the vehicle's center of mass. The result is that, even if the vehicle is orbiting a perfectly spherical primary, the mass center does not follow a truly Keplerian orbit, on account of the extended body inertia distribution. Conversely, when the spacecraft orbits a planet with a non-spherical gravitational distribution (i.e., resulting in asphericity measurable in terms of J_2 and J_3 effects), the orbit in general will be elliptic, and the line of nodes will in general move in space. In particular, the longitude of the ascending node, the mean anomaly, and the argument of perigee will change with time. The result is that the attitude dynamics of the vehicle is coupled to the orbital dynamics. The modeled time variations of mean anomaly, longitude of ascending node, and argument of perigee are as follows Ref. 4:

$$\begin{aligned} \dot{M} &= \Omega [1 + 1.5 J_2 (R_p/a)^2] (1 - 1.5 \sin^2 i) / (1 - e^2)^{3/2} \\ \dot{\Omega}_L &= -1.5 J_2 \Omega (R_p/a)^2 \cos i / (1 - e^2)^2 \\ \dot{\omega}_p &= +1.5 J_2 \Omega (R_p/a)^2 (2 - 2.5 \sin^2 i) / (1 - e^2)^2 \end{aligned} \quad (15)$$

At each time step, the eccentric anomaly E is found by solving Kepler's equation $E - M = e \sin(E)$. The true anomaly can then be found as $\nu = \text{atan2}(\sin(E)\sqrt{1-e^2}, \cos(E)-e)$. The current radius is $R = a[1 - e \cos(E)]$. The components of \mathbf{R}_0 in the inertial frame are then:

$$\mathbf{R}_0 = \Phi_I^T |\mathbf{R}_0| \begin{pmatrix} \cos(\omega_p + \nu) \cos\Omega_L - \sin(\omega_p + \nu) \sin\Omega_L \cos i \\ \cos(\omega_p + \nu) \sin\Omega_L + \sin(\omega_p + \nu) \cos\Omega_L \cos i \\ \sin(\omega_p + \nu) \sin i \end{pmatrix} \quad (16)$$

Defining the colatitude $\delta = \text{asin}(z/|\mathbf{R}_0|)$, the inertial vectors of the acceleration of the vehicle due to higher order gravitational potential terms (J_2, J_3) can also be written as:

$$\mathbf{a}_{J_2} = -\frac{3}{2} \frac{\mu J_2}{|\mathbf{R}_0|^5} \begin{bmatrix} x(1-5\sin^2\delta) & y(1-5\sin^2\delta) & z(3-5\sin^2\delta) \end{bmatrix} \Phi_I \quad (17)$$

$$\mathbf{a}_{J_3} = -\frac{5}{2} \frac{\mu J_3}{|\mathbf{R}_0|^6} \begin{bmatrix} x(3-7\sin^2\delta)\sin\delta & y(3-7\sin^2\delta)\sin\delta & z(6-7\sin^2\delta)\sin\delta - 3|\mathbf{R}_0|/5 \end{bmatrix} \Phi_I \quad (18)$$

In the simplified case in which the vehicle is approximated as a dumbbell constrained to librate in the orbital plane only, the fully coupled nonlinear equations of motion in the orbital radius R_0 , the true anomaly η , and the pitch angle α become as follows Ref. 1:

$$\text{Radius: } \ddot{R}_0 - \dot{\eta}^2 R_0 = -\frac{\mu}{R_0^2} \left[1 + \frac{3}{2mR_0^2} (\text{trace}(J) - 3J_1 \sin^2 \alpha - 3J_3 \cos^2 \alpha) \right] - \frac{f}{m} \cos(\alpha + \theta) \quad (19)$$

$$\text{True Anomaly: } \ddot{\eta} + 2 \frac{\dot{R}_0}{R_0} \dot{\eta} = -\frac{3\mu}{mR_0^5} (J_3 - J_1) \sin \alpha \cos \alpha - \frac{f}{mR_0} \sin(\alpha + \theta) \quad (20)$$

$$\text{Pitch Angle: } \ddot{\alpha} - \dot{\eta} = \frac{3\mu}{R_0^3} \frac{(J_3 - J_1)}{J_2} \sin \alpha \cos \alpha + \frac{f}{J_2} (d_3 \sin \theta - d_1 \cos \theta) \quad (21)$$

where f is the applied thrust, d_1 and d_3 are the components of the thrust application point in the spacecraft body frame, θ is the thrust direction angle in body frame. We have assumed that the spacecraft body frame is a principal axis frame. From the last three equations, one can observe that:

- the equations of motion are nonlinear and non-homogeneous.
- the equations of motion apply to any type of orbit, including spiral-in/out phases.
- the attitude dynamics and the orbital dynamics are, indeed, coupled through the pitch angle α , which is not necessarily small, and through the true anomaly.
- the fact that the orbit is eccentric is reflected in the true anomaly rates. When the orbit is circular, the attitude dynamics is uncoupled from the orbital dynamics.
- the thrust direction and magnitude affect both the orbital and attitude dynamics. The applied thrust is a “follower” force (i.e. it follows the motion of the vehicle in its own body frame), and the thrust vector is not necessarily directed along one of the body axes only.
- the gravity gradient effect (represented by the terms in $s\alpha$ and $c\alpha$) appears in all the equations.

These interaction effects are shown in Figure 6 and Figure 7 where, for a typical 152 km altitude eccentric and regressive orbit around Europa (hence J_2 effects are taken into account), the pitch response is shown to depend slightly on the orbital inclination, more strongly on the eccentricity, and even more strongly on the orbital altitude, as expected. To conclude this section, one might think that the attitude-orbit coupling is a totally negligible effect in most situations. However, because of the low-thrust dynamics, all the attitude maneuvers have durations comparable with the orbital

period of a low altitude science orbit around one of Jupiter's moons (~ 2 hours). This fact alone singles out the need to further investigate this interaction.

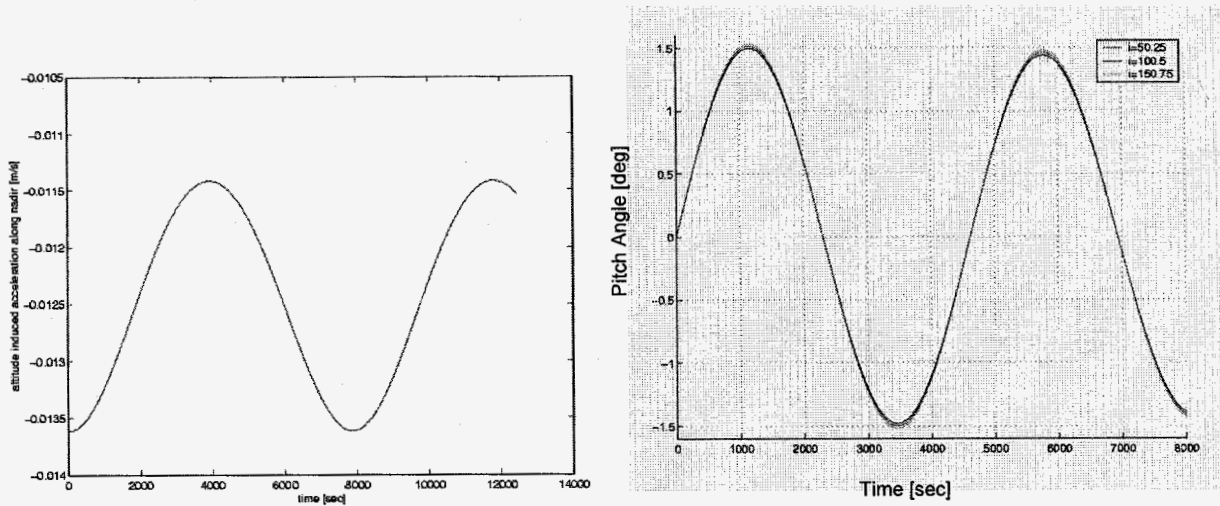


Figure 6. Left: Spacecraft linear orbital acceleration induced by attitude dynamics for a typical 152 km altitude orbit around Europa. Right: Spacecraft Pitch angle vs. orbital inclination for a typical 152 km altitude orbit around Europa.

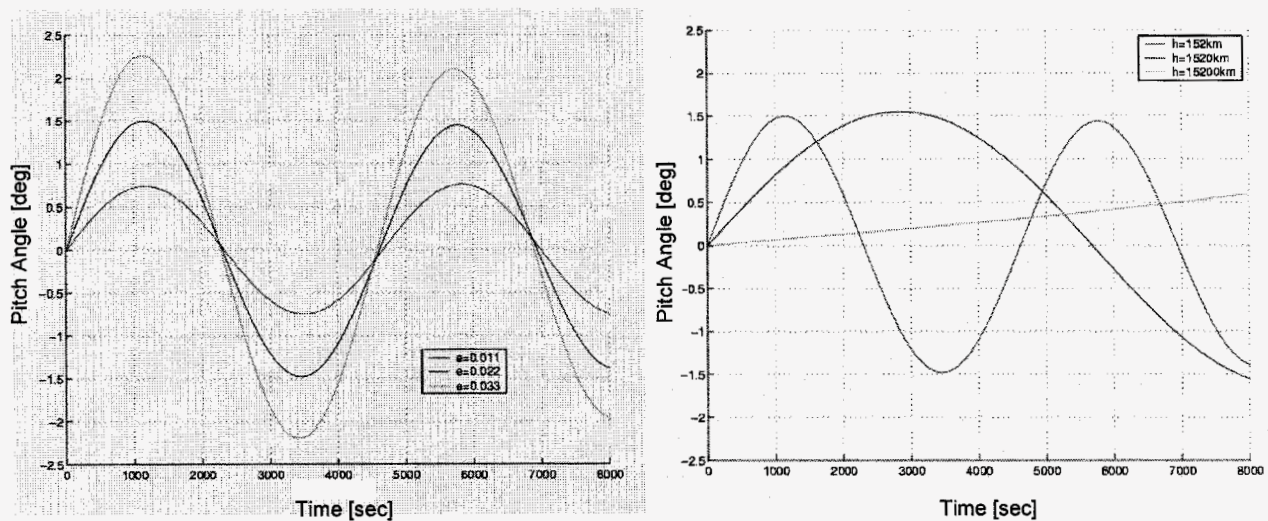


Figure 7. Left: Spacecraft Pitch angle vs. orbital eccentricity for a typical 152 km altitude orbit around Europa. Right: Spacecraft Pitch angle vs. orbital altitude for an orbit around Europa.

Interaction between the flexible spacecraft dynamics and the pointing control loops

In this section we make some analytical considerations on the JIMT flexible multibody dynamics, and on the interaction of the flexibility with the articulation controller.

Models for JIMT Controls Structure Interaction

Figure 8 shows a simplified model capturing effects of flexibility on JIMT pointing dynamics. The characteristic Equation for Euler Beam with Tip Mass and Inertia, and clamped-free boundary conditions is [Ref. 2]:

$$\begin{aligned} &\lambda^4 [1 - \cos(\lambda\ell) \cosh(\lambda\ell)] + \lambda \left(\frac{m_1 \omega^2}{EI} \right) [\sin(\lambda\ell) \cosh(\lambda\ell) - \cos(\lambda\ell) \sinh(\lambda\ell)] + \\ &\lambda^3 \left(\frac{J_1 \omega^2}{EI} \right) [\cos(\lambda\ell) \sinh(\lambda\ell) + \sin(\lambda\ell) \cosh(\lambda\ell)] + \\ &m_1 J_1 \left(\frac{\omega^2}{EI} \right)^2 [1 + \cos(\lambda\ell) \cosh(\lambda\ell)] = 0 \end{aligned} \quad (22)$$

where $\lambda^4 = \frac{\rho A \omega^2}{EI}$ and the following i -th mode admissible function $\phi_i(x)$ satisfies the geometric and boundary conditions of a clamped-free appendage:

$$\phi_i(x) = 1 - \cos\left(\frac{i\pi x}{\ell}\right) + \frac{1}{2}(-1)^{i+1} \left(\frac{i\pi x}{\ell}\right)^2 \quad (23)$$

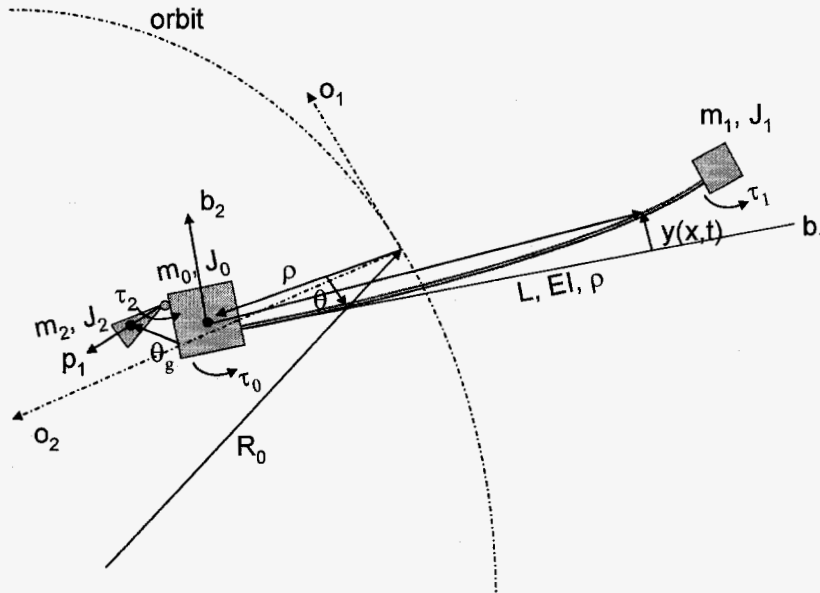


Figure 8. Simplified model capturing effects of flexibility on JIMT pointing dynamics.

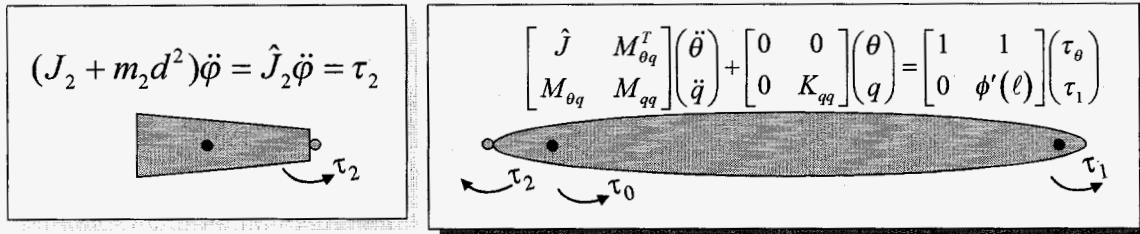


Figure 9. Equilibrium of flexible base body with attached articulation.

Clamped-free boundary conditions were chosen on account of m_0 (~20,000 kg) being much greater than m_1 (~5000 kg). The physical displacement is computed via separation of variables as a summation over the number of modes

as $y(x, t) = \sum_{i=1}^N \phi_i(x) q_i(t)$. Using Lagrange's equations, we obtain:

$$\begin{bmatrix} \hat{J} & M_{\theta q}^T \\ M_{\theta q} & M_{qq} \end{bmatrix} \begin{pmatrix} \ddot{\theta} \\ \ddot{q} \end{pmatrix} + \begin{bmatrix} 0 & 0 \\ 0 & K_{qq} \end{bmatrix} \begin{pmatrix} \theta \\ q \end{pmatrix} = \begin{bmatrix} 1 & 1 \\ 0 & \phi'(\ell) \end{bmatrix} \begin{pmatrix} \tau_0 \\ \tau_1 \end{pmatrix} \quad (24)$$

where

$$\hat{J} = J_0 + 2[J_1 + m_1(r + \ell)^2] + 2 \int_0^\ell \rho(r + x)^2 dx \quad (25)$$

$$(M_{\theta q})_i = J_1 \phi_i'(\ell) + m_1(r + \ell) \phi_i(\ell) + \int_0^\ell \rho(r + x) \phi_i(x) dx \quad (26)$$

$$(M_{qq})_{ij} = J_1 \phi_i'(\ell) \phi_j'(\ell) + m_1 \phi_i(\ell) \phi_j(\ell) + \int_0^\ell \rho \phi_i(x) \phi_j(x) dx \quad (27)$$

$$(K_{qq})_{ij} = \int_0^\ell EI \phi_i''(x) \phi_j''(x) dx \quad (28)$$

These equations of motion may be summarized as

$$M_a \ddot{X}_a + K_a X_a = D_a U_a \quad (29)$$

For one mode only, we have:

$$\begin{aligned} \hat{J} &= J_h + 2\rho L(r^2 + rL + L^2/3) + 2[m_1(r+L)(r+L) + J_1] \\ M_{\theta\theta} &= \rho L^2(0.5 + 2/\pi^2 + \pi^2/8) + \rho rL(1 + \pi^2/6) + m_1(r+L)(2 + \pi^2/2) + J_1 \pi^2/L \\ \phi'(L) &= \pi^2/L \\ M_{qq} &= \rho L(3 + \pi^2/3 + \pi^4/20 + 0.5) + m_1[1 + (1 + \pi^2/2)]^2 + J_1 \pi^4/L^2 \\ K_{qq} &= 1.5 EI \pi^4/L^3 \end{aligned}$$

Through solving the eigenvalue problem:

$$\begin{aligned} K_a \Phi_a &= \Lambda_a M_a \Phi_a \\ \Phi_a^T M_a \Phi_a &= 1 \end{aligned} \quad (30)$$

and introducing the canonical transformation $X_a = \Phi_a \eta_a$, where $\Phi_a = [\Phi_1 \ \dots \ \Phi_n]$ and there are $n < N$ retained modes, we obtain:

$$\ddot{\eta}_a + \Lambda_a^2 \eta_a = \Phi_a^T D_a U_a \quad (31)$$

These are the modal dynamics equations with gimbal locked if M_a includes the gimbal inertia. Introducing now the structural damping matrix Σ , we may write:

$$\dot{Z}_a = \begin{bmatrix} 0 & 1 \\ -\Lambda_a^2 & -2\Sigma\Lambda_a \end{bmatrix} \begin{pmatrix} \eta_a \\ \dot{\eta}_a \end{pmatrix} + \begin{bmatrix} 0 \\ \Phi_a^T D_a \end{bmatrix} U_a = A_a Z_a + B_a U_a \quad (32)$$

The observation equations are $Y_a = [\Phi_a \quad \Phi_a] Z_a$. We also have:

$$\varphi = \theta + \alpha \quad (33)$$

where φ is the inertial gimbal angle, θ the inertial spacecraft attitude angle, and α is the gimbal angle relative to the spacecraft. Figure 9 depicts this interaction, and the Newton-Euler scheme used to represent the system's equations of motion when the articulated payload is present. Figure 5 showed the natural frequencies of the flexible spacecraft with rotors locked. Figure 10, 11, and 12 depict the open loop transfer functions from force and torque excitation at the reactor to the angles at the SC bus location along the roll (x), pitch (y), and yaw (z) directions, assuming a 2% modal damping uniformly distributed to all the modes. Because this is a non-collocated sensor-actuator problem, significant intervening flexibility appears in the resulting transfer functions. In particular, we may observe the lead effect caused by a zero preceding the remaining flexible poles of the system, which may be the cause of instability if the controller is designed in such a way to ignore this interaction.

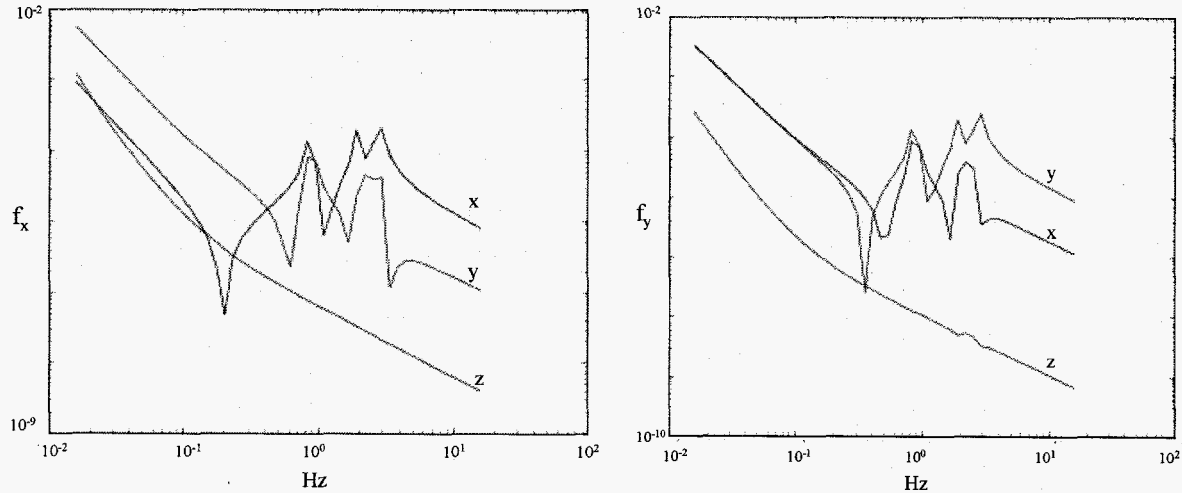


Figure 10. Left: Open loop transfer functions from X-force excitation at reactor to angles at SC bus [N vs. Hz]. Right: Open loop transfer functions from Y-force excitation at reactor to angles at SC bus [N vs. Hz].

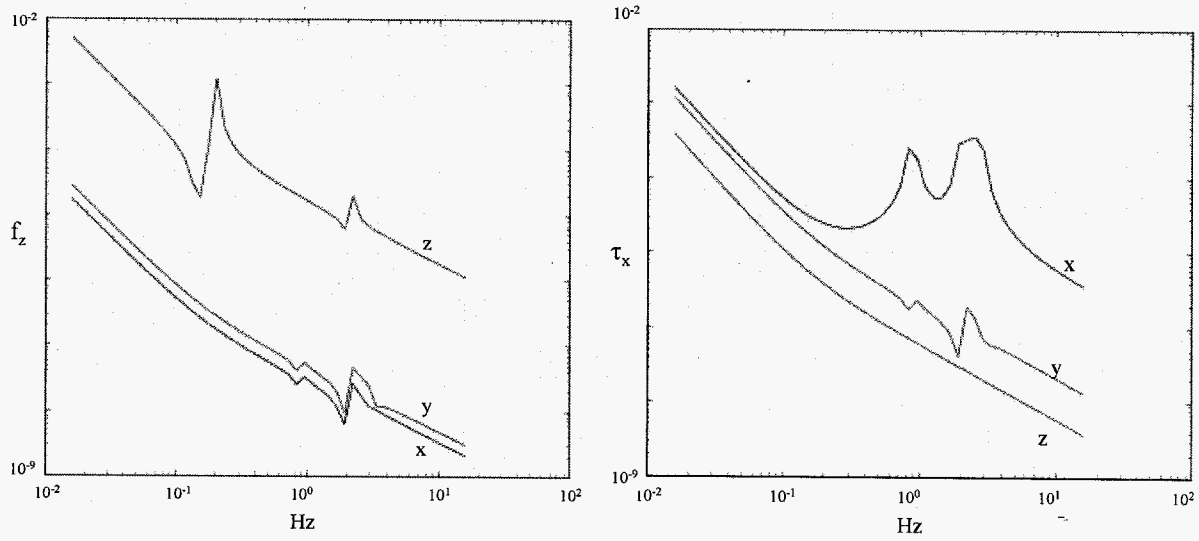


Figure 11. Left: Open loop transfer functions from Z-force excitation at reactor to angles at SC bus [N vs. Hz]. Right: Open loop transfer functions from X-torque excitation at reactor to angles at SC bus [Nm vs. Hz].

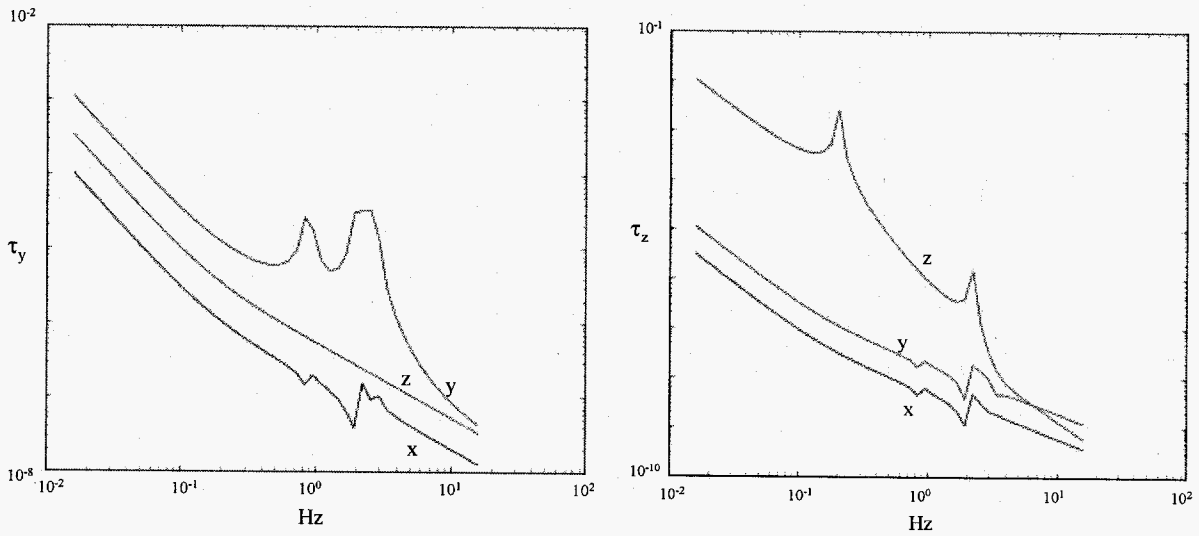


Figure 12. Left: Open loop transfer functions from Y-torque excitation at reactor to angles at SC bus [Nm vs. Hz]. Right: Open loop transfer functions from Z-torque excitation at reactor to angles at SC bus [Nm vs. Hz].

From Figure 9, we obtain:

$$\begin{bmatrix} \hat{J} & M_{\theta q}^T & 0 \\ M_{\theta q} & M_{qq} & 0 \\ 0 & 0 & \hat{J}_2 \end{bmatrix} \begin{bmatrix} \ddot{\theta} \\ \ddot{q} \\ \ddot{\phi} \end{bmatrix} + \begin{bmatrix} 0 & 0 & 0 \\ 0 & K_{qq} & 0 \\ 0 & 0 & 0 \end{bmatrix} \begin{bmatrix} \theta \\ q \\ \phi \end{bmatrix} = \begin{bmatrix} 1 & 1 & -1 \\ 0 & \phi'(\ell) & 0 \\ 0 & 0 & 1 \end{bmatrix} \begin{bmatrix} \tau_0 \\ \tau_1 \\ \tau_2 \end{bmatrix} \quad (34)$$

and, in compact form:

$$M_a \ddot{X}_b + K_a X_b = D_a U_b \quad (35)$$

Through the eigenvalue problem:

$$\begin{aligned} K_b \Phi_b &= \Lambda_b M_b \Phi_b \\ \Phi_b^T M_b \Phi_b &= 1 \end{aligned} \quad (36)$$

and introducing the canonical transformation $X_b = \Phi_b \eta_b$, we obtain:

$$\ddot{\eta}_b + \Lambda_b^2 \eta_b = \Phi_b^T D_b U_b \quad (37)$$

These are the modal dynamics equations with gimbals free. Introducing the damping matrix Σ , we have:

$$\dot{Z}_b = \begin{bmatrix} 0 & 1 \\ -\Lambda_b^2 & -2\Sigma\Lambda_b \end{bmatrix} \begin{pmatrix} \eta_b \\ \dot{\eta}_b \end{pmatrix} + \begin{bmatrix} 0 \\ \Phi_b^T D_b \end{bmatrix} U_b = A_b Z_b + B_b U_b \quad (38)$$

together with the observation equations:

$$Y_b = \begin{bmatrix} \Phi_b & \Phi_b \end{bmatrix} Z_b \quad (39)$$

We assume from now on that we are retaining only one flexible mode. Using a tilde to denote a Laplace-transformed variable, we write the equations of motion in the frequency domain as:

$$\begin{aligned} \begin{pmatrix} \tilde{\theta} \\ \tilde{q} \\ \tilde{\alpha} \end{pmatrix} &= \begin{bmatrix} \hat{J}_s^2 & M_{\theta q}^T s^2 & 0 \\ M_{\theta q} s^2 & M_{qq} s^2 + K_{qq} & 0 \\ \hat{J}_2 s^2 & 0 & \hat{J}_2 s^2 \end{bmatrix}^{-1} \begin{bmatrix} 1 & 1 & -1 \\ 0 & \phi'(\ell) & 0 \\ 0 & 0 & 1 \end{bmatrix} \begin{pmatrix} \tilde{\tau}_0 \\ \tilde{\tau}_1 \\ \tilde{\tau}_2 \end{pmatrix} \\ &= \begin{bmatrix} b_{\theta\theta} & b_{\theta q} & b_{\theta\varphi} \\ b_{q\theta} & b_{qq} & b_{q\varphi} \\ b_{\varphi\theta} & b_{\varphi q} & b_{\varphi\varphi} \end{bmatrix} \begin{pmatrix} \tilde{\tau}_0 \\ \tilde{\tau}_1 \\ \tilde{\tau}_2 \end{pmatrix} \end{aligned} \quad (40)$$

If we now observe the spacecraft's inertial attitude angle (through a star tracker, for example) and the articulation relative angle (through a gimbal mounted resolver, for example), we have:

$$Y = \varphi = \begin{bmatrix} 1 & 0 & \dots & 0 & 1 \end{bmatrix} \begin{pmatrix} \tilde{\theta} \\ \tilde{q} \\ \tilde{\alpha} \end{pmatrix} = \begin{bmatrix} 1 & 0 & \dots & 0 & 1 \end{bmatrix} \begin{bmatrix} b_{\theta\theta} & b_{\theta q} & b_{\theta\varphi} \\ b_{q\theta} & b_{qq} & b_{q\varphi} \\ b_{\varphi\theta} & b_{\varphi q} & b_{\varphi\varphi} \end{bmatrix} \begin{pmatrix} \tilde{\tau}_0 \\ \tilde{\tau}_1 \\ \tilde{\tau}_2 \end{pmatrix} \quad (41)$$

We can then write the bus dynamics equation as:

$$\tilde{\theta} = b_{\theta\theta} \tilde{\tau}_0 + b_{\theta q} \tilde{\tau}_1 + b_{\theta\varphi} \tilde{\tau}_2 \quad (42)$$

where:

$$b_{\theta\theta} = -\frac{1}{s^2} \left[\frac{M_{qq}s^2 + K_{qq}}{(M_{\theta q}^2 - \hat{J}M_{qq})s^2 - \hat{J}K_{qq}} \right] \quad (43)$$

is the platform to bus transfer function,

$$b_{\theta\phi} = \frac{1}{s^2} \left[\frac{M_{qq}s^2 + K_{qq}}{(M_{\theta q}^2 - \hat{J}M_{qq})s^2 - \hat{J}K_{qq}} \right] \quad (44)$$

is the spacecraft to bus transfer function,

$$b_{\theta q} = \frac{1}{s^2} \left[\frac{(\phi'(\ell)M_{\theta q} - M_{qq})s^2 - K_{qq}}{(M_{\theta q}^2 - \hat{J}M_{qq})s^2 - \hat{J}K_{qq}} \right] \quad (45)$$

is the reactor to bus transfer function. Similarly, the relative gimbal dynamics equation can be derived as:

$$\tilde{\alpha} = b_{\phi\theta}\tilde{\tau}_0 + b_{\phi q}\tilde{\tau}_1 + b_{\phi\phi}\tilde{\tau}_2 \quad (46)$$

where:

$$b_{\phi\theta} = \frac{1}{s^2} \left[\frac{M_{qq}s^2 + K_{qq}}{(M_{\theta q}^2 - \hat{J}M_{qq})s^2 - \hat{J}K_{qq}} \right] \quad (47)$$

is the spacecraft to platform transfer function,

$$b_{\phi\phi} = \frac{1}{s^2} \left[\frac{1}{\hat{J}_2} - \frac{M_{qq}s^2 + K_{qq}}{(M_{\theta q}^2 - \hat{J}M_{qq})s^2 - \hat{J}K_{qq}} \right] \quad (48)$$

is the gimbal to platform transfer function, and

$$b_{\phi q} = \frac{1}{s^2} \left[\frac{(M_{qq} - \phi'(\ell)M_{\theta q})s^2 + K_{qq}}{(M_{\theta q}^2 - \hat{J}M_{qq})s^2 - \hat{J}K_{qq}} \right] \quad (49)$$

is the reactor to platform transfer function. These transfer function expressions show how the effect of the flexibility of the base body appears in the pointing control loop, and the deviation from the transfer function of a second order integrator is apparent. In particular, one may note that for certain combinations of parameters, a pole-zero cancellation may occur, in which case actuating the gimbal has no effect on the inertial pointing response.

Flexible body interactions with gimbal servo-controller.

In general, there are three basic types of interaction between a gimbal servo-controller and intervening flexibility (Figure 13):

- *Base-body Flexibility* (compliance in structure): unstable if the control bandwidth approaches resonance.
- *In-the-loop Flexibility* (compliance between sensor and actuation in servo): unstable.
- *Appendage Flexibility* (compliance outboard of the sensor package): almost always stable.

All three types have similar effects on gimbal servo's performance. They limit the pointing control bandwidth. Since controller bandwidth is in relation with the ability of the control system to reject disturbances, flexibility effects limit the controller performance capability. One can observe that pointing stability performance degrades with decreasing control bandwidth. In-the-loop flexibility is generally the most destabilizing effect. What this means is that the controller bandwidth should be kept at least an order of magnitude away from the significant structural modes. In general, by increasing structural damping, or using notch filters or high-performance controllers, modes can be tolerated within the controller bandwidth but at the expense of complexity of implementation. Also, high-performance controllers rely on detailed knowledge of the structural resonances. As a rule-of-thumb, if structural resonances migrate, performance degrades. This brings the need for sophisticated methods for on-board system identification. The transfer function of a rigid system (double integrator filter) can be written as $G_{rigid} = y_j / u_i = j\text{-th sensor}/i\text{-th actuator} = 1/Js^2$. An example of this is the attitude dynamics of a rigid spacecraft. The transfer function of a flexible system can instead be written as $G_{rigid+flex} = G_{rigid} + \gamma_{ij}$ where $\gamma_{ij} = (\phi_i^k \phi_j^k / m_k) / (s^2 + 2\xi_k \omega_k s + \omega_k^2)$. An example of this is the attitude dynamics in one axis with boom appendage. This is the case of JIMT.

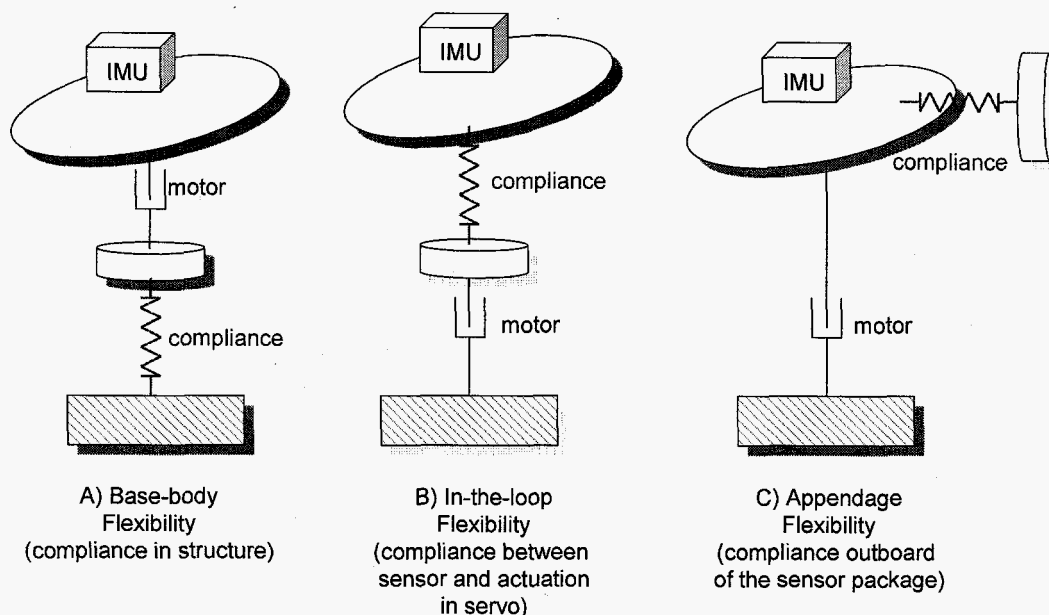


Figure 13. Flexible body interactions with gimbal servo-controller.

We conclude this section with some qualitative considerations. Gain margin can be defined as the amount of gain of a system that can be increased (decreased) before it goes unstable. Phase margin can be defined as the amount of phase of a system that can be decreased (increased) before it goes unstable. Phase margin affects the response of the closed loop system. The controller bandwidth is approximately the crossover frequency of the closed-loop transfer function. For a 2nd order system with roll-off well above the flexible mode, the resonance is phase-stabilized. Gain and Phase margin are modest. For JIMT, if the controller bandwidth is well above flexible mode (i.e., closing the loop on the Scanplatform while JIMT behaves as a noodle), there is enough control authority for the platform to not be disturbed by the noodle and still do its pointing well. In the limit, the scan platform is stand-alone in free space. The system can still be pointed. For a 2nd order system with roll-off well below the flexible mode, the resonance is gain-stabilized. Gain and Phase margin are modest. For JIMT, if the controller bandwidth is well below flex. mode (i.e., closing the loop on the JIMT base-body attitude while the Ion engine pod booms are flexing), the high frequency boom dynamics does not have enough inertia to react to the control action, hence their effect on the attitude is minor. The system can still be pointed. For a 2nd order system with roll-off in the vicinity of the flexible mode, negative margins result since gain

margin is high near phase crossover, and phase margin is high near gain crossover. This is why modal resonances have to be away from controller bandwidth. For JIMT: if the controller bandwidth is close to flex. mode (i.e., closing the loop on the scan-platform at a rate commensurate with one of the base-body frequencies), the stability margins are adverse, and hurt the pointing. The system cannot be pointed. Additional complications arise when the structural modes are clustered, or when additional system modes need to be included, such as sloshing modes.

Slew into Nadir-pointed attitude using thrusters

A simulation was run for the case in which the spacecraft is commanded to carry out a 90 degree turn from the “along-track” attitude held during the spiral-in phase into Europa, into the nadir pointed attitude required to point the scan platform, located at the rear of the spacecraft bus, towards the moon. This is shown in Figure 14. This maneuver fights the gravity gradient induced on the spacecraft by the moon at a 152 km altitude, and is carried out by actuating the hydrazine thrusters causing a pure couple about the spacecraft’s center of mass. The simulation program models the following effects: Europa orbit with generic orbital elements; SC as a rigid body; Structural flexibility; coupled orbital and attitude propagators; Environmental perturbation forces and torques (J_2 , J_3 , gravity gradient); Actuators: thrusters, reaction wheels; Sensors: gyro, accel, star tracker. The state vector is: inertial position and velocity, quaternion, angular velocities, momentum of reaction wheels. Inputs (thruster and RW forces and torques) are applied in body frame, whereas outputs are: position, velocity and acceleration related inertial and orbiting reference frames; quaternion and rates in body frame. The simulation assumed that the RCS proportional hydrazine thrusters are been actuated with the following characteristics: specific impulse $I_{sp}=2500$ Ns/kg, 1N max. thrust, translation deadbands of 1mm in position and $30 \mu\text{m/s}$ in velocity, and rotational deadbands of $150 \mu\text{rad}$ in attitude and $5 \mu\text{rad/s}$ in attitude rate. The thrust resolution (or thruster quantization level) was assumed to be of $1 \mu\text{N}$, and the thrust noise (with an uncertainty level of 1σ) equal to $0.1 \mu\text{N}$. The variance of star tracker measurement noise (1σ) is 3 arc-sec. The variance of gyro measurement noise (1σ) is 3 arc-sec. The variance of the gyro angle random walk (ARW) is $0.07 \text{ deg/hr}^{1/2}$. The standard deviation of the gyro bias drift is 1.0 deg/hr (100 s correlation time), and the variance of the accelerometer measurement noise is $35 \mu\text{g}$. A proportional-derivative controller is used to slew the vehicle. The attitude control bandwidth is taken to be 0.07 Hz. The attitude control gain is $0.1892 [\text{s}^2/\text{rad}]$, and the attitude rate control gain is $0.4398 [\text{s}^3/\text{rad}]$.

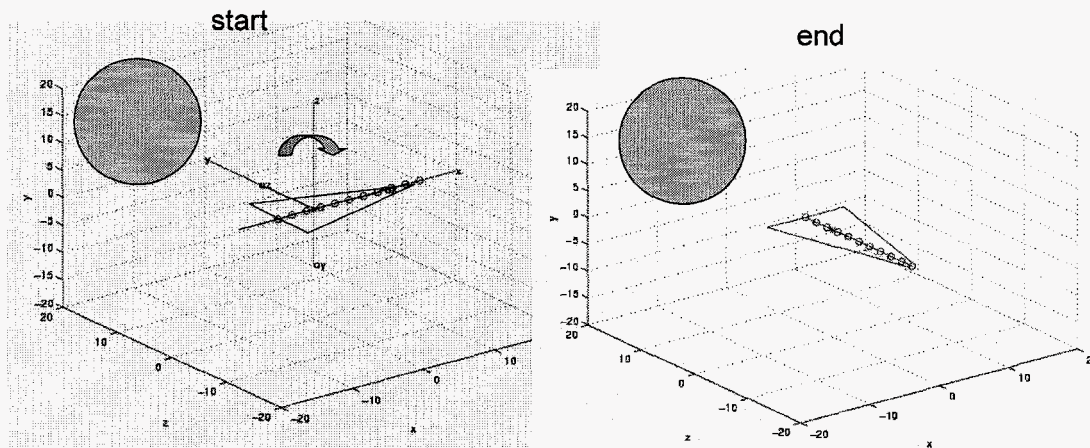


Figure 14. A 90 degree slew about the orbit normal to reach the nadir pointed attitude around Europa.

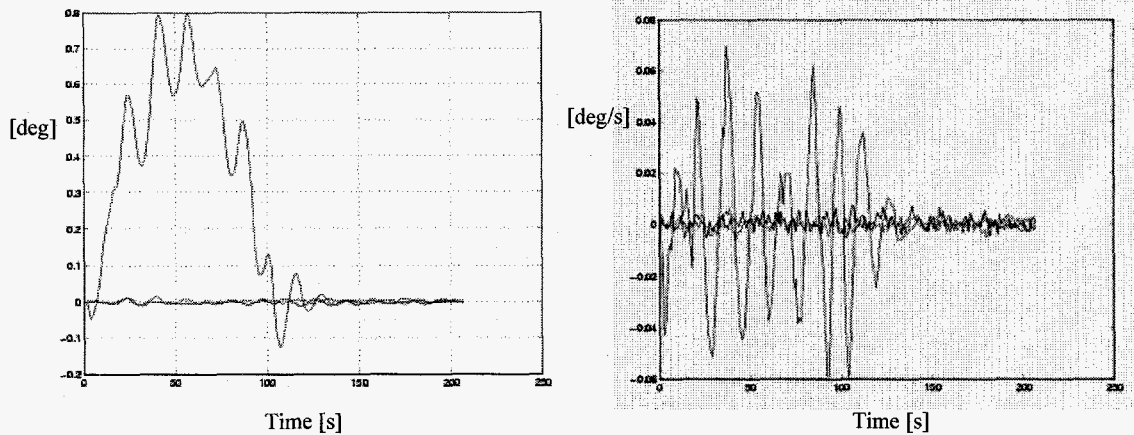


Figure 15. Attitude error (deg) and Attitude rate error (deg/s) during slew as a function of time.

Figure 15 shows the attitude and attitude rate errors in tracking the slew command. A very small residual oscillation is left at the end of the maneuver (approximately within 0.01 degs and 0.005 deg/s). This oscillatory response may not be small enough for the science observation phase to begin, and reaction wheels will have to be used for precision pointing while in the gravity gradient field of Europa.

Conclusions

In this paper we have described some of the dynamics and control challenges presented by the Jovian Moon Tour spacecraft as conceived for the 2002 study. The JIMT spacecraft presents challenging attitude-orbital and controls-structure interactions. This paper has summarized some of these dynamical effects. The attitude-orbit coupling is motivated by the need of the low-thrust propulsion system to follow complex orbital trajectories. The control-structure coupling is caused by having to accurately point the existing multiple articulated payloads while mounted on a large flexible base. A simulation model has been described which is capable of handling the complex orbital and attitude dynamics arising during the spiraling maneuvers of the spacecraft, as well as potential interactions between the spacecraft flexibility and the inertial pointing of the articulations. The initial numerical simulations demonstrate that some of the challenges hitherto identified in the areas of flexible body dynamics and gravity-gradient stabilization can be faced via computational analysis, and reasonably accurate assessments of the pointing performance can be made.

Acknowledgements

This research was carried out at the Jet Propulsion Laboratory, California Institute of Technology, under a contract with the National Aeronautics and Space Administration. The authors are grateful to Dr. Tooraj Kia and Mr. Duncan MacPherson for useful technical discussions.

References

- [1] Hughes, P.C., *Spacecraft Attitude Dynamics*, Prentice Hall, 1986.
- [2] Junkins, J.L. and Kim, Y., *Introduction to Dynamics and Control of Flexible Structures*, AIAA Education Series, 1993.
- [3] Stuhlinger, E.: *Ion Propulsion for Space Flight*, McGraw-Hill, 1964.
- [4] Vallado, D.: *Fundamentals of Astrodynamics and Applications*, The McGraw-Hill Companies, Inc., 1997.

End of File

